Monthly Notices of the ROYAL ASTRONOMICAL SOCIETY

MNRAS **476,** 1624–1636 (2018) doi:10.1093/mnras/sty275

Cosmic clocks: a tight radius–velocity relationship for H I-selected galaxies

Gerhardt R. Meurer,[1★] Danail Obreschkow,[1] O. Ivy Wong,[1,2★] Zheng Zheng,[3] Fiona M. Audcent-Ross[1] and D. J. Hanish[4]

[1]*International Centre for Radio Astronomy Research, The University of Western Australia, 35 Stirling Highway, Crawley, WA 6009, Australia*
[2]*ARC Centre of Excellence for All-sky Astrophysics (CAASTRO), Building A28, School of Physics, The University of Sydney, NSW 2006, Australia*
[3]*National Astronomical Observatories, Chinese Academy of Sciences, A20 Datun Road, Chaoyang District, Beijing 100012, China*
[4]*Spitzer Science Center, California Institute of Technology, MC 220-6, 1200 E California Blvd., Pasadena, CA 91125, USA*

Accepted 2018 January 29. Received 2018 January 14; in original form 2017 May 22

ABSTRACT

H I-selected galaxies obey a linear relationship between their maximum detected radius $R_{\rm max}$ and rotational velocity. This result covers measurements in the optical, ultraviolet, and H I emission in galaxies spanning a factor of 30 in size and velocity, from small dwarf irregulars to the largest spirals. Hence, galaxies behave as clocks, rotating once a Gyr at the very outskirts of their discs. Observations of a large optically selected sample are consistent, implying this relationship is generic to disc galaxies in the low redshift Universe. A linear radius–velocity relationship is expected from simple models of galaxy formation and evolution. The total mass within $R_{\rm max}$ has collapsed by a factor of 37 compared to the present mean density of the Universe. Adopting standard assumptions, we find a mean halo spin parameter λ in the range 0.020–0.035. The dispersion in λ, 0.16 dex, is smaller than expected from simulations. This may be due to the biases in our selection of disc galaxies rather than all haloes. The estimated mass densities of stars and atomic gas at $R_{\rm max}$ are similar ($\sim$0.5 $M_\odot$ pc^{-2}), indicating outer discs are highly evolved. The gas consumption and stellar population build time-scales are hundreds of Gyr, hence star formation is not driving the current evolution of outer discs. The estimated ratio between $R_{\rm max}$ and disc scalelength is consistent with long-standing predictions from monolithic collapse models. Hence, it remains unclear whether disc extent results from continual accretion, a rapid initial collapse, secular evolution, or a combination thereof.

Key words: galaxies: dwarf – galaxies: fundamental parameters – galaxies: kinematics and dynamics – galaxies: spiral – galaxies: structure.

1 INTRODUCTION

Based on the cold dark matter (CDM) scenario for galaxy evolution, the main structural and dynamical properties of galaxies' haloes and discs are expected to obey simple virial scaling relations (Fall & Efstathiou 1980; Mo, Mao & White 1998; Dutton et al. 2007). These properties are typically specified as a radius R, rotation velocity amplitude V, and a mass M, or alternatively luminosity L as a proxy for mass. For haloes in virial equilibrium, we expect $V \propto R \propto M^{1/3}$ (Mo et al. 1998, hereafter MMW98). Although the dark matter (DM) is not directly observable, scaling relations are observed in the properties of the *baryons*, although the slopes (power-law exponents) of the relations are not exactly as predicted for the haloes (e.g. Courteau et al. 2007).

The most used scaling relation is the velocity–luminosity relation, better known as the Tully–Fisher relation (hereafter TFR; Tully & Fisher 1977), and similarly the Baryonic TFR (McGaugh et al. 2000), which is a velocity–mass relationship. Baryonic physics is messy. The scaling between luminosity and baryonic mass depends on the star formation history, which varies between galaxies (Grebel 1997; Tolstoy, Hill & Tosi 2009; Weisz et al. 2011; Williams et al. 2011), the initial mass function (IMF), which also apparently varies between galaxies whether they are dominated by young stellar populations (Hoversten & Glazebrook 2008; Lee et al. 2009; Meurer et al. 2009; Gunawardhana et al. 2011) or old ones (Treu et al. 2010; Cappellari et al. 2012; Conroy & van Dokkum 2012; Dutton, Mendel & Simard 2012; Smith, Lucey & Carter 2012; van Dokkum & Conroy 2012), and the dust content and distribution (Calzetti, Kinney & Storchi-Bergmann 1994; Gordon et al. 2001; Tuffs et al. 2004). Theory and observations indicate that feedback from star formation (Governato et al. 2010; Oh et al. 2011) or active galactic nuclei (e.g. Bonoli et al. 2016) can rearrange the distribution

★ E-mail: gerhardt.meurer@icrar.org (GRM); ivy.wong@icrar.org (OIW)

of baryons, and in the process drag along the DM into an altered distribution, affecting all scaling relations.

The radius–velocity (*RV*) relationship has received somewhat less attention. Courteau et al. (2007) and Dutton et al. (2007) fit scaling relations to R, V, and L in a sample of luminous spiral galaxies having optical spectroscopic observations. They found that the scatter in the *RV* relationship was the highest compared to the *LV* and *RL* relationships. Some of the scatter in the *RV* relation is due to the uncertainties and ambiguities of measuring R. This includes lack of a uniform definition of radial scalelength (cf. Pohlen & Trujillo 2006), contamination by the bulge component, selection effects (especially with surface brightness), and errors due to dust. However, if instead of using a scalelength to characterize R we consider an outer radius, then some of these concerns (e.g. bulge and dust) are minimized and a tighter relationship can be found. This will allow a better measurement of the intrinsic scatter in the *RV* relationship, which is very sensitive to the spin of the haloes in which galaxies lie (e.g. Mo et al. 1998; Courteau et al. 2007; Dutton et al. 2007; Obreschkow & Glazebrook 2014).

Here, we demonstrate a nearly linear *RV* relationship in various measurements of H I-selected galaxy samples. In Section 2, we present our primary samples and detail the measurements we use. Section 3 shows the observed correlations and quantifies the slopes and scatters; we also test the results on a large comparison sample selected and measured in the optical giving consistent results. In Section 4, we show what a linear *RV* relation means in the context of CDM-dominated galaxy evolution models. Our results are discussed further in Section 5, where we estimate the spin parameter of galaxies, the properties of discs near their outer extents, and then discuss how these results relate to ideas on what limits the extent of galaxy discs. Our conclusions are presented in Section 6.

2 SAMPLES AND MEASUREMENTS

We measure the *RV* relationship in three primary samples. The first uses optical data from the Survey of Ionization in Neutral Gas Galaxies (SINGG; Meurer et al. 2006), which is an Hα and R-band follow-up survey to the H I Parkes All Sky Survey (HIPASS; Koribalski et al. 2004; Meyer et al. 2004; Zwaan et al. 2004) combined with single dish H I data from HIPASS. The second uses data from the Survey of Ultraviolet emission in Neutral Gas Galaxies (SUNGG; Wong 2007), which observed HIPASS-selected galaxies in the ultraviolet (UV) with *GALEX*, for a sample largely overlapping with SINGG. Here, we use sub-samples of SINGG and SUNGG designed to ensure that reasonable rotation amplitudes can be derived from the HIPASS H I data. Specifically, both samples are selected to have major to minor axial ratios $a/b \geq 2$ and to be the only apparent star-forming galaxy in the system. The a/b cut guarantees a minimum inclination of about 60°, thus limiting projection errors in calculating orbital velocities. For those galaxies observed by SINGG, the isolation criterion was determined using the Hα images, which are roughly the same size as the HIPASS beam. For those SUNGG galaxies not observed by SINGG, isolation was determined morphologically; systems with companions of similar angular size, obvious signs of interaction, or noted as interacting with another galaxy in the literature were excluded. These selection criteria result in 71 and 87 galaxies from SINGG and SUNGG, respectively, with an overlap of 47 galaxies in common. The third sample uses H I imaging data of the 20 galaxies studied by Meurer, Zheng & de Blok (2013, hereafter MZD13).

In all three samples, H I data are used to infer the maximum rotation amplitude. The implicit assumption is that the H I in these galaxies is dominated by a rotating disc. It is important to bear in mind that the selection of the samples requires detectable amounts of H I, and thus is biased against gas-poor disc galaxies (e.g. S0 galaxies and ellipticals). Note that the a/b cut applied to the SINGG and SUNGG samples also is likely to remove early type and S0 galaxies from our samples. As pointed out by Meurer et al. (2006), very few such galaxies are found in the SINGG sample. The selection against early type galaxies may have implications on the types of haloes they are associated with, as discussed in Section 5.1. As we show below, the implied rotational amplitudes range from $\sim$10 km s^{-1} (dwarf galaxies) to $\sim$300 km s^{-1} (the largest spirals).

The radii used for the SINGG and SUNGG samples depend on the *maximum* extent of the galaxies observed in the optical and UV, respectively. Both surveys are designed to measure the total light of extended nearby galaxies using a series of concentric elliptical annuli. For SINGG, the apertures are set in a manner slightly modified from that given in Meurer et al. (2006). As noted there, the aperture shape (a/b and position angle) and centre are set by eye to include all the apparent optical emission. In most cases, this shape matches well the apparent shape of the galaxy in the R band, i.e. a tilted disc. We then grow the apertures to an arbitrarily large size, and determine, by eye, where the raw (*before* sky subtraction) radial surface brightness profile levels off. The surface brightness of the galaxy at that radius is on the order of 1 per cent of the sky brightness.

The radius where the raw surface brightness profiles flatten is called the maximum radius $R_{\rm max}$. Since the R-band light almost always can be traced further than Hα, $R_{\rm max}$ typically measures the maximum detectable extent in the optical continuum. Most exceptions are dwarf galaxies with strong minor-axis outflows. Optical sizes were estimated in this manner by two of us. First by DH and then by GRM, who 'tweaked' the size estimates in about half of the SINGG sample. Typically those that were adjusted were made larger because the raw profiles indicated that a small amount of additional flux could be gained doing so. Here, we use the tweaked aperture radii. Compared to using the initial estimates, the use of the tweaked apertures increases $R_{\rm max}$ by 0.06 dex on average and also reduces the scatter in the residuals of the fits described below by 0.06 dex (when taken in quadrature). The SUNGG maximum radius is set in a similar manner; it is determined separately in near-ultraviolet (NUV) and far-ultraviolet (FUV), and the maximum of the two is taken as $R_{\rm max}$.

For both the SINGG and SUNGG samples, we interpolate enclosed flux versus aperture semi-major axis profiles to determine the radii containing 50 per cent (R_{50}) and 90 per cent (R_{90}) of the flux in the R band and UV, respectively.

For the MZD13 sample, we use three radii: $R_{\rm max}$ is the maximum extent of the H I radial profiles as given in the original studies used by MZD13, whereas R_1 and R_2 represent the extent of the region of the H I surface mass density profile $\Sigma_{\rm H\,I}$ fitted with a power law by MZD13. These radii are set by eye to mark kinks in the H I radial profiles, indicating changes of slope in $\log(\Sigma_{\rm H\,I}(R))$. On average, they are close to the radii that contain 25 per cent and 75 per cent of the H I flux, respectively (MZD13). Unfortunately, neither MZD13 nor the studies they employed calculated R_{50} and R_{90} for the H I data.

The shape of the rotation curve (hereafter RC) $V(R)$ of galaxies varies systematically with mass, or peak rotational velocity, from nearly solid body (linearly rising), for the lowest mass galaxies, to RCs that are flat at nearly all radii, or even slightly declining at large R for the most massive galaxies (Persic & Salucci 1991; Persic, Salucci & Stel 1996; Catinella, Giovanelli & Haynes 2006). Unless stated otherwise, we take V to be the maximum rotational amplitude. For most cases, this will be the amplitude at the flat part of the RC. In

the majority of other cases, it will be the farthest measured point of the RC. We take these definitions to be synonymous. For the SINGG and SUNGG samples, we derive V from the full width at half-maximum of the H I spectrum from HIPASS, assuming a flat RC over all relevant radii. We follow the method of Meyer et al. (2008) and correct the line widths for inclination, and broadening resulting from turbulence, relativity, instrumental effects, and data smoothing. As with Meyer et al. (2008) the inclinations are derived from a/b. For the H I sample we interpolate the RCs, from the various original studies used by MZD13 to arrive at rotation amplitudes at R_1, R_2, and $R_{\rm max}$ separately (i.e. $V(R_1)$, $V(R_2)$, and $V(R_{\rm max})$).

3 RESULTS

3.1 Observed correlations

We show the observed correlations separately for each data set in three figures. Fig. 1 shows the RV relationship for the SINGG optical data. In the left-hand panel, the y-axis gives the radius as $R_{50}(R)$, i.e. the radius containing 50 per cent of the R-band light; similarly the middle panel shows $R_{90}(R)$ as the radius; whereas the right-hand panel uses $R_{\rm max}$ as defined from the SINGG optical data. The velocity in all panels is the circular velocity V defined from the HIPASS H I line widths (Section 2). Similarly, Fig. 2 shows R_{50}(NUV), R_{90}(NUV), and $R_{\rm max}$ from the SUNGG UV data in the left-hand, middle, and right-hand panels, respectively, against V derived from HIPASS. Fig. 3 shows the H I radii R_1, R_2, and $R_{\rm max}$ plotted against the circular velocities interpolated at those radii $V(R_1)$, $V(R_2)$, and $V(R_{\rm max})$ in the left-hand, middle, and right-hand panels, respectively.

We fit the RV relations in log–log space as

$$\log(R) = \alpha + \beta \log(V) \quad (1)$$

using an ordinary linear least squares bisector algorithm (Isobe et al. 1990) weighting each point equally, and iteratively clipping points that deviate from the fit by more than three times the dispersion in R. Table 1 reports the results of the fits, giving the coefficients α, β, the dispersion of the residuals $\sigma_{\log(R)}$, $\sigma_{\log(V)}$, and Pearson's correlation coefficient r_{xy}. Some of these quantities are also listed in Figs 1–3.

For the optical and UV samples, the fits are the 'best' at $R_{\rm max}$, where best is defined as having the highest r_{xy} and lowest $\sigma_{\log(R)}$ and $\sigma_{\log(V)}$. For the H I sample, the fit at R_1, marking where the H I profiles flatten, is much worse than the other two fits. The flattening is likely to be due to the increasing dominance of molecular gas at small radii (Bigiel et al. 2008; Leroy et al. 2008). The fits at R_2 and $R_{\rm max}$ have similar scatters, indistinguishable statistically. In summary, the fits are their best, or close to it, at $R_{\rm max}$, where β is close to but slightly greater than unity, that is, a linear relationship.

A linear RV implies that the orbital time

$$t_{\rm orb} = \frac{2\pi R}{V} \quad (2)$$

is constant (assuming the orbit shape is well approximated by a circle). We list the mean $\log(t_{\rm orb})$ in Table 1 and in the panels of Figs 1–3. The RV relation at $R_{\rm max}$ is nearly identical in the three figures even though $R_{\rm max}$ is defined at very different wavelengths, which are sensitive to different physical processes. Fig. 4 a overplots the three samples at $R_{\rm max}$, showing the excellent correspondence in the RV relationships. They all imply that $t_{\rm orb} \approx 1$ Gyr, with a scatter of 0.14–0.18 dex (38 per cent to 51 per cent). Thus, H I-selected disc galaxies behave like clocks and rotate once in a Gyr at their outermost detected radii. This holds for galaxies which range in radius from $R_{\rm max} \sim 1.5$ kpc, having $V \sim 10\,{\rm km\,s^{-1}}$ to those with $R_{\rm max} \sim 50$ kpc and $V \sim 300\,{\rm km\,s^{-1}}$. The RV relationship for $t_{\rm orb} = 1$ Gyr is shown with the dashed line in Fig. 4a.

The SINGG–RV relation is equally well defined at R_{50}, R_{90}, and $R_{\rm max}$. However, the meaning is less clear when using R_{50} and R_{90}. The velocity used, V, is determined from the line width of integrated H I velocity profiles of galaxies that are spatially unresolved. The H I in galaxies typically is weighted to larger radius than the easily observed optical emission (e.g. Leroy et al. 2008), hence the derived V is also applicable to large radii. The rotation amplitude at R_{90} and R_{50} will be systematically overestimated using V as one goes to lower rotation amplitudes and shorter radii (i.e. the effect will be stronger for R_{50} than R_{90}). Hence, if we used the true V values at R_{90} and R_{50} then we should see shallower β values than shown in Fig. 1.

The RV relations in the UV also are defined using H I velocity profiles. Here, we see significantly larger $\sigma_{\log(R)}$ residuals when using R_{50} and R_{90} as well as steeper β values compared to the RV relation at $R_{\rm max}$. We posit that the worse fits are due to whether or not galaxies have a central starburst, and the degree to which they are affected by dust. These will have more of an impact on the distribution of the UV luminosity at small radii than in the determination of $R_{\rm max}$.

3.2 Results for a comparison sample

Our primary results are for three samples having H I-based V measurements, one has H I-based R measurements, and two have overlapping selections based on H I properties. In order to address whether our results may be a byproduct of working with H I data, we now consider a sample that is selected and measured in the optical; the sample of 698 disc galaxies of Zheng et al. (2015). The sample was selected from the Pan-STARRS1 (PS1) Medium Deep Survey (Chambers et al. 2016) fields, and measured from the stacked survey images. The galaxies were selected to have images in all PS1 bands (g, r, i, z, y), spectroscopic redshifts from SDSS-III, [1] to be fairly face-on ($a/b < 2$), and to be well resolved with a Petrosian (1976) radius[2] $R_{\rm P} > 5$ arcsec. Galaxy profiles are then measured to $2R_{\rm P}$. This algorithm recovers ≥ 94 per cent of the total light for galaxies having a Sérsic (1963) index $n \leq 2$ typical of disc galaxies (Graham et al. 2005). Zheng et al. (2015) found that radial surface brightness profiles typically show a 'break', or change in slope, in the bluer bands with the break less apparent towards longer wavelengths. They fitted stellar population models to annular photometry in the five bands to derive stellar mass density profiles and integrated to yield the total stellar mass. They recorded R_{50}, R_{90}, and the break radius $R_{\rm b}$ all measured in the r band. Hence, as with the other samples, we have three fiducial radii to work with. Instead of using a measured rotational velocity, we use $V_{\rm c}'$, the circular velocity estimated from the stellar mass based TFR of Reyes et al. (2011). This fit to the TFR has been shown to well represent the kinematics of an SDSS based sample (Simons et al. 2015) that has redshifts similar to this PS1 sample.

The resulting RV' relationships are shown in Fig. 5. We fit this sample in the same manner as done for the other samples (Section 3.1). The fit parameters are tabulated in Table 1. In all

[1] http://skyserver.sdss.org/

[2] where the local surface brightness is 20 per cent of the average interior surface brightness.

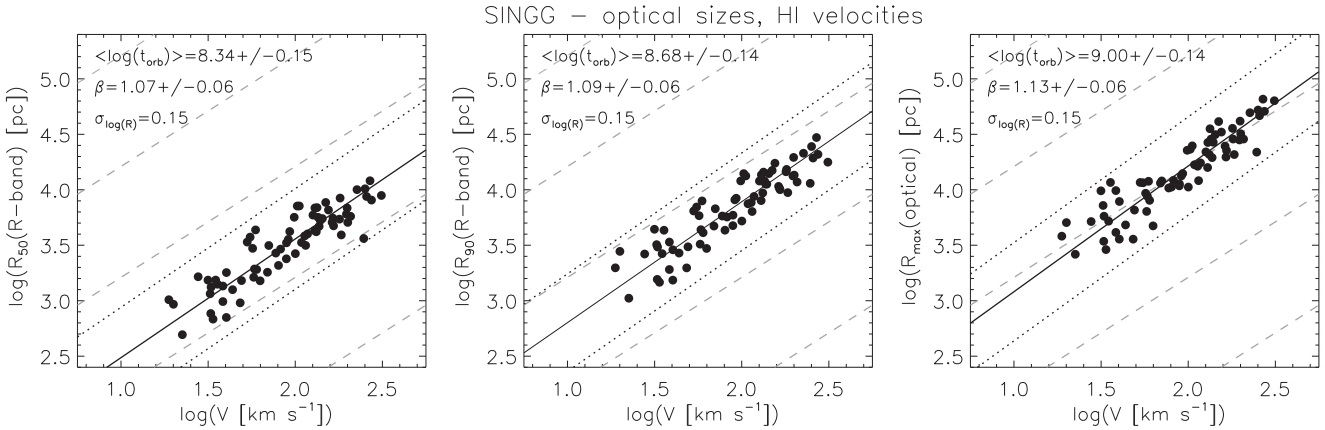

Figure 1. Radius R plotted against circular velocity V on a logarithmic scale as derived from SINGG optical data. The radii plotted in the left-hand, middle, and right-hand panels are $R_{50}(R)$, $R_{90}(R)$, and $R_{\rm max}$(optical), respectively, whereas all three panels plot the same HIPASS H I based V. The solid line shows the iteratively clipped ordinary least squares bisector fit to the plotted quantities, whereas the dotted line shows the fit offset by $\pm 3\sigma_{\log(R)}$, where $\sigma_{\log(R)}$ is the dispersion of the R residuals. Each panel is annotated with the mean log orbital time, $\langle \log(t_{\rm orb}) \rangle$, and its dispersion (after clipping), the fitted slope β and its error, and the rms of the residuals in the ordinate. The parallel grey dashed lines from the bottom to top show where $t_{\rm orb} = 10^{8}$, $10^{8.5}$, $10^{9.0}$, $10^{9.5}$, and 10^{10} years, respectively.

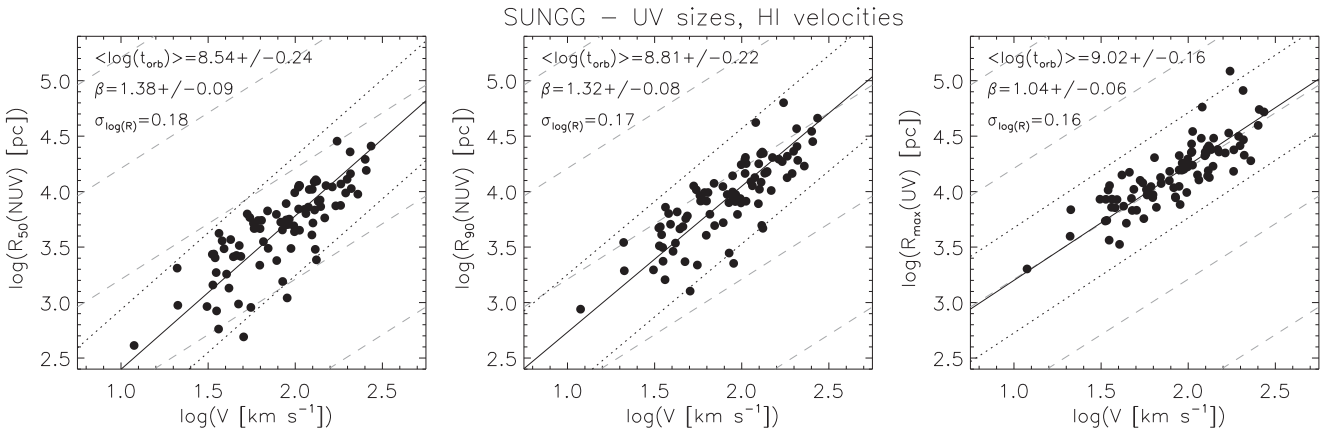

Figure 2. Radius R plotted against circular velocity V on a logarithmic scale as derived from SUNGG UV data. The radii used here are R_{50}(NUV), R_{90}(NUV), and $R_{\rm max}$(UV) in the left-hand, middle and right-hand panels, respectively. The meanings of the various lines and annotations are the same as in Fig. 1.

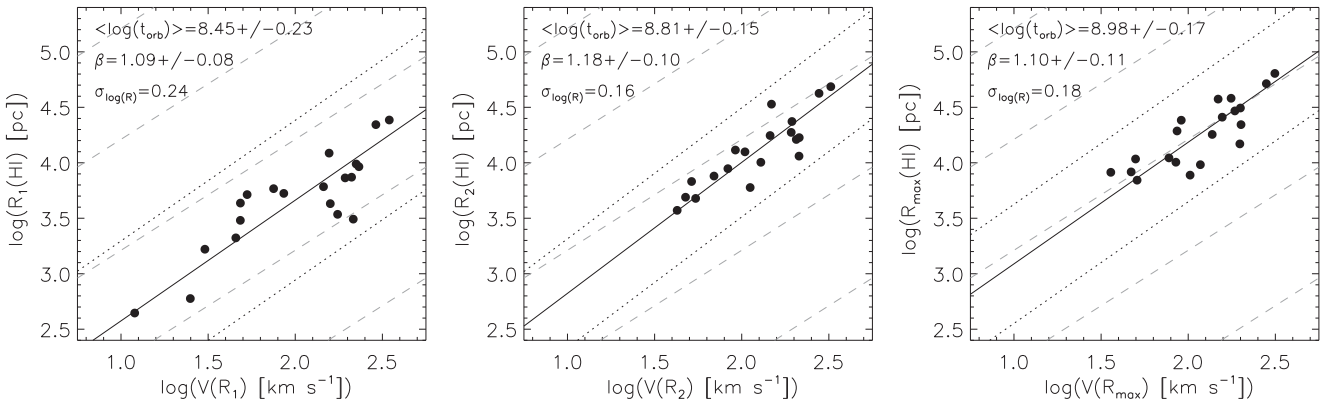

Figure 3. Radius R plotted against circular velocity V on a logarithmic scale for the H I sample of MZD13. The radii R_1 (left-hand panel) and R_2 (centre panel) delimit the region where the H I surface brightness profile is a power law with index $\gamma \approx -1$ (see MZD13 for details), whereas $R_{\rm max}$ (right-hand panel) is the maximum detected extent of H I. The meanings of the various lines and annotations are the same as in Fig. 1.

Table 1. Fit parameters.

Sample (1)	Radius (2)	N_{used} (3)	N_{rej} (4)	α (5)	β (6)	log (t_{orb}) (7)	$\sigma_{\log(R)}$ (8)	$\sigma_{\log(V)}$ (9)	r_{xy} (10)
SINGG	$R_{50}(R)$	71	0	1.42 ± 0.12	1.07 ± 0.06	8.34 ± 0.15	0.15	0.14	0.899
SINGG	$R_{90}(R)$	71	0	1.71 ± 0.12	1.09 ± 0.06	8.68 ± 0.14	0.15	0.14	0.908
SINGG	R_{max}(opt)	71	0	1.95 ± 0.12	1.13 ± 0.06	9.00 ± 0.14	0.15	0.13	0.914
SUNGG	R_{50}(NUV)	88	0	1.11 ± 0.11	1.33 ± 0.08	8.54 ± 0.22	0.18	0.24	0.797
SUNGG	R_{90}(NUV)	88	0	1.56 ± 0.15	1.24 ± 0.08	8.81 ± 0.21	0.18	0.22	0.805
SUNGG	R_{max}(UV)	87	1	2.16 ± 0.12	1.04 ± 0.06	9.02 ± 0.16	0.16	0.16	0.830
H I	R_1(H I)	20	0	1.49 ± 0.15	1.09 ± 0.08	8.45 ± 0.23	0.24	0.22	0.859
H I	R_2(H I)	19	1	1.64 ± 0.19	1.18 ± 0.10	8.81 ± 0.15	0.16	0.14	0.876
H I	R_{max}(H I)	20	0	1.99 ± 0.24	1.10 ± 0.11	8.98 ± 0.17	0.18	0.16	0.825
PS1	$R_{50}(r)$	692	6	1.32 ± 0.07	1.07 ± 0.03	8.26 ± 0.13	0.14	0.13	0.770
PS1	$R_b(r)$	694	4	1.41 ± 0.07	1.14 ± 0.03	8.52 ± 0.14	0.15	0.13	0.761
PS1	$R_{90}(r)$	689	9	1.68 ± 0.06	1.07 ± 0.03	8.62 ± 0.12	0.12	0.11	0.818

Column (1): the galaxy sample fitted. Column (2): the radius measured. Column (3): the number of data points used in the fit. Column (4): the number of data points rejected from the fit. Column (5): the zeropoint of the fit. Column (6): the slope of the fit. Column (7): average log of the orbital time of the fitted data points. Column (8): dispersion in the log of the residuals in radius R of the fitted points. Column (9): dispersion in the log of the residuals in orbital velocity V of the fitted points (or implied orbital velocity V' for the PS1 sample). Column (10): Pearson's correlation coefficient using all data points.

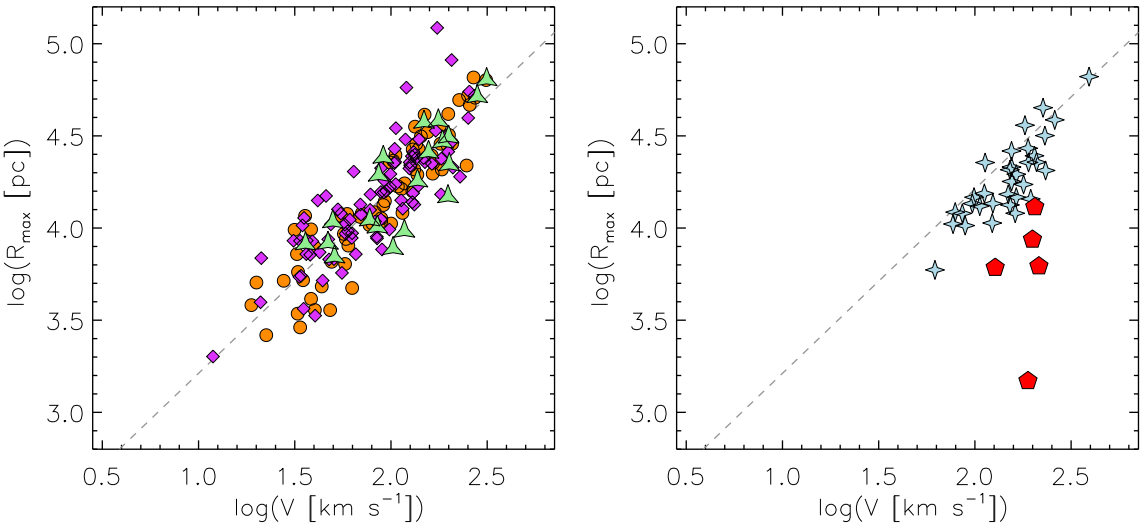

Figure 4. Maximum radius R_{max} plotted against circular velocity V on a logarithmic scale for our combined primary samples is shown in the left-hand panel. Here, orange circles, purple diamonds, and green triangles show the SINGG, SUNGG, and H I samples displayed in Figs 1c, 2c, and 3c, respectively. In the right-hand panel, we show other estimates of the maximum disc size compared to rotational amplitude. In the right-hand panel, the blue four pointed stars show the optically determined R_{max} of edge-on galaxies for the sample of Kregel, van der Kruit & de Grijs (2002) against their V. The red pentagons show the H II region truncation radius R_{HII} plotted against V for galaxies in common between the samples of Martin & Kennicutt (2001) and MZD13. The grey dashed line in both panels shows the relationship expected for $t_{orb} = 1$ Gyr.

three cases, the fits to the PS1 data are nearly linear ($\beta \approx 1$), with the fit at R_{90} being closest to linear and having the smallest scatter $\sigma_{\log(R_{90})} = 0.12$ dex of any of our RV fits.

Amongst the PS1 sample fits, the one at R_b has the largest scatter, 0.15 dex in $\sigma_{\log(R_b)}$, and deviates the farthest from linear ($\beta = 1.12$). Nevertheless, the scatter about the mean orbital time of 0.13 dex compares well with the other RV fits. The larger scatter compared to the fit at R_{90} may arise because the strength of the radial profiles breaks is highly variable with some galaxies 'breaking down' (more typical), others 'breaking up', and some showing no discernible breaks (Freeman 1970; Pohlen & Trujillo 2006; Zheng et al. 2015).

The (logarithmic) mean t_{orb} at R_{50} and R_{90} for the PS1 sample 0.18, 0.42 Gyr, respectively, is close to that for the SINGG sample 0.22, 0.48 Gyr. Meanwhile, at R_b, the mean $t_{orb} = 0.36$ Gyr, intermediate between those at R_{50} and R_{90}. Hence, $R_b \approx 1.8R_{50} \approx 0.8R_{90}$ for the PS1 sample. Although Zheng et al. (2015) do not measure R_{max}, they note that typically $R_{90} = R_P$ and that most of the light is recovered at $2R_P$, hence we expect $R_{max} \approx 2R_{90}$ for the PS1 sample. For flat RCs, then we infer that $t_{orb}(R_{max}) = 2t_{orb}(R_{90}) = 0.83$ Gyr for the PS1 sample, within 0.08 dex of the SINGG sample. The t_{orb} estimates for the PS1 sample at R_{50}, R_{90} and that implied at R_{max} are all lower than those for the SINGG sample, suggesting a more general optical selection of galaxies may result in smaller galaxies than an H I selection. However, the differences are all close to or about equal to the 0.06 dex systematic error noted in Section 2. Hence, to that level of accuracy, the same RV relationship for H I selected galaxies applies to all disc galaxies at low redshifts.

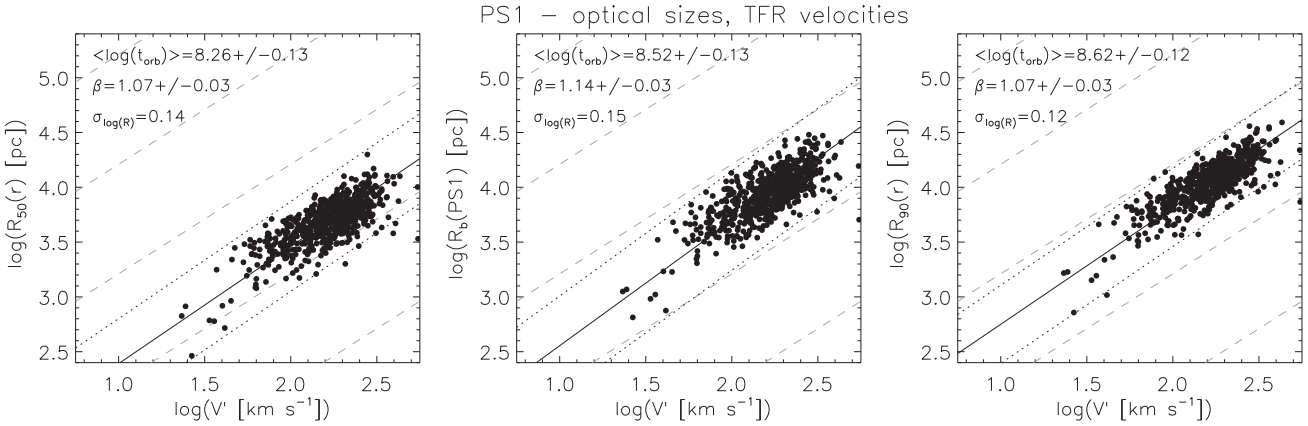

Figure 5. Radius R plotted against estimated circular velocity V' on a logarithmic scale for the Pan-STARRS1 sample of Zheng et al. (2015). Here, V' is not a direct measurement of circular velocity, but estimated from the stellar mass based TFR of Reyes et al. (2011). The radii used here are the radius containing 50 per cent of the PS1 r-band light $R_{50}(r)$), the break radius $R_{\rm b}$(PS1), and the radius containing 90 per cent of the r-band light $R_{90}(r)$ in the left-hand, middle and right-hand panels, respectively. The meanings of the various lines and annotations are the same as in Fig. 1.

The somewhat tighter fits to the PS1 sample does not necessarily mean that the intrinsic scatter in the *RV* relations is lower than for the SINGG sample. This is because an inferred rather than measured velocity is used. Since the V' in Fig. 5 is derived from luminosities, these are essentially *RL* or $RM_\star$ correlations we are showing. Saintonge & Spekkens (2011) find a very tight *RL* relation (having a scatter of 0.05 dex in R) using their SFI++ sample of spiral galaxies, and employing isophotal radii and I-band luminosities. Similarly, both Courteau et al. (2007) and Hall et al. (2012) find smaller scatters in their *RL* relations than their *VR* relations. In part, this is because errors in L are effectively reduced by a factor of 3–4 due to the TFR scaling, making them competitive or better than velocity errors (Saintonge & Spekkens 2011). Velocities are also more prone to errors in inclination, position angle, and non-circular motions. Working with stellar mass (fitted to photometry), as done with our PS1 sample, also improves the accuracy by effectively spreading any error over five bands and weighting the results to the reddest bands. But improved accuracy may not be the only cause for the tight fits in Fig. 5. Saintonge & Spekkens (2011) performed a careful error analysis of the scatter in their scaling relations and estimate the intrinsic scatter in their *RL* relations (∼0.034 dex in R) is less than half of that in their *RV* relations (∼0.084 dex in R).

4 EXPECTATIONS FROM SIMPLE GALAXY EVOLUTION MODELS

A constant $t_{\rm orb}$ at $R_{\rm max}$ implies a constant spherically averaged mean mass (baryons and DM) density ρ interior to $R_{\rm max}$ since

$$\rho = \frac{3\pi}{G t_{\rm orb}^2}, \tag{3}$$

where G is the gravitational constant. Our adopted $t_{\rm orb}(R_{\rm max}) = 1$ Gyr yields the mean mass density interior to $R_{\rm max}$:

$$\langle \rho(R_{\rm max}) \rangle = 2.1 \times 10^{-3}\, \mathcal{M}_\odot\, {\rm pc}^{-3}. \tag{4}$$

The closure density of the Universe, ρ_c, is given by

$$\rho_c = \frac{3H_z^2}{8\pi G}, \tag{5}$$

where H_z is the redshift (z) dependent Hubble constant. This can be used to estimate the collapse factor of matter within $R_{\rm max}$. Adopting $H_0 = 70\,{\rm km\,s^{-1}\,Mpc^{-1}}$ and the results of the Planck Collaboration (Planck Collaboration XVI 2014) that the ratio of the cosmic matter density to the closure density $\Omega_{\rm M} = 0.315$, we have

$$\frac{\langle \rho(R_{\rm max}) \rangle}{\Omega_{\rm M} \rho_c} = 49000. \tag{6}$$

The third root of this is the average collapse factor $f_{\rm c}(R_{\rm max})$ of the matter within $R_{\rm max}$ compared to the present day matter density of the Universe:

$$\langle f_{\rm c}(R_{\rm max}) \rangle = 36.6. \tag{7}$$

The 'virial radius' R_{200} is usually defined as the radius where the mean density of the enclosed mass is 200 times larger than ρ_c. From equation (5), it is apparent that ρ_c depends only on redshift, and thus, by definition, a linear *RV* relationship is expected at R_{200} at any given epoch given by equation (2) of MMW98:

$$R_{200} = \frac{V}{10 H_z}. \tag{8}$$

From equation (2), the orbital time at the virial radius at the present epoch is $t_{\rm orb} = 8.8$ Gyr.

The RC interior to R_{200} depends on the distribution of DM and baryons. MMW98 used an analytical approach to examine the expected structure of disc galaxies within DM haloes under a variety of plausible assumptions about cosmogeny and distribution of the baryons and DM. They adopt a simple isothermal sphere to parametrize DM haloes, and show that this framework is convenient for understanding how the galaxy scaling relations are influenced by the properties of their haloes. Adopting this approach, MMW98 derived equation (8). An isothermal sphere has a flat (constant) RC and a density profile

$$\rho(R) = \frac{V^2}{4\pi G R^2}. \tag{9}$$

A flat RC is well supported observationally in most disc galaxies, especially at large radii (e.g. Rubin, Thonnard & Ford 1978; Bosma 1981; Mathewson, Ford & Buchhorn 1992; de Blok et al. 2008; Epinat et al. 2008), whereas the shape of the inner part of the RC varies systematically with mass, or V (e.g. Persic & Salucci 1991; Catinella et al. 2006). Since our results are the most consistent at $R_{\rm max}$, where RCs are typically flat, the isothermal approximation suffices for our purposes. For a pure exponential disc galaxy in a dominant isothermal halo, MMW98 derive the disc scalelength $R_{\rm d}$

relative to R_{200} in their equation (12). Combining that with equation (8) yields

$$R_{\rm d} = \frac{V}{\sqrt{200}H_z}\left(\frac{j_{\rm d}}{m_{\rm d}}\right)\lambda, \quad (10)$$

where $j_{\rm d}$ is the fraction of the total angular momentum in the disc, $m_{\rm d}$ is the fraction of the total mass in the disc, and λ is the spin parameter. For systems that are not purely exponential discs in an isothermal halo, the scalefactor ($1/[\sqrt{200}H_z]$) will vary depending on the detailed distributions of DM and baryons (MMW98). Thus, a linear relationship between $R_{\rm d}$ and V should exist if $(j_{\rm d}/m_{\rm d})\lambda$ is constant.

If the DM and baryons are well mixed when galaxies collapse, one would naively expect $j_{\rm d} = m_{\rm d}$ and thus a constant $j_{\rm d}/m_{\rm d}$ (MMW98). This is also the working assumption of Fall & Efstathiou (1980), whose simple models were consistent with the observations of the time. Although it is impossible to observationally confirm this expectation because of the invisible nature of DM, simulations allow it to be tested. Posti et al. (2018), using a similar approach to ours, and matching of galaxy properties to halo properties from a variety of recent cosmological N-body simulations find that $j_{\rm d}/m_{\rm d}^{2/3}$ is approximately constant, close to what all we require. We note that a constant $j_{\rm d}/m_{\rm d}$ is difficult to reproduce in more detailed numerical simulations (Governato et al. 2010). The dependence of λ on mass and other parameters for dark haloes, as measured in numerous simulations, is also weak (e.g. MMW98; Cole & Lacey 1996; Bett et al. 2007; Macciò et al. 2007). Thus, naive considerations tell us that we expect a linear RV relation when a disc scalelength, or anything proportional to it, is used to measure size. This would be the case for the isophotal sizes of pure exponential discs that have constant central surface brightness as originally proposed by Freeman (1970).

Disc galaxies, however, are not that simple. They typically contain a bulge increasingly apparent with morphological type (e.g. Hubble 1926). Since Freeman's landmark work, it has become apparent that discs obey a surface brightness–luminosity relationship (e.g. Kauffmann et al. 2003), and that the radial profiles frequently show breaks from being pure exponential (Freeman 1970; Pohlen & Trujillo 2006; Zheng et al. 2015). However, allowing for these complications may not necessarily cause major changes to the RV relation. MMW98 derive the behaviour of an exponential disc in a halo having the typical profile found in CDM-only simulations (Navarro, Frenk & White 1997, hereafter NFW), which is allowed to respond to the disc's mass. They find relationships for $R_{\rm d}$ and the maximum rotational velocity that differ from the isothermal case by form functions that depend on $j_{\rm d}$, $m_{\rm d}$, λ, and halo concentration c. Of these, c is the parameter that is expected to have the largest impact (Dutton et al. 2007). For example, MMW98 considered the case of a bulge plus disc embedded in an NFW halo, and found that disc size depends on assumptions about angular momentum transfer between the bulge, disc, and halo. They found that disc sizes can vary by a factor of about 2, whereas maximum velocities only vary by $\lesssim 20$ per cent.

5 DISCUSSION

The formalism presented in Section 4 allows us to place our results in a cosmological context. We continue with this approach in Section 5.1 by examining the constraints on the spin parameter λ and its dispersion implied by our results. Section 5.2 discusses what our results imply for the properties at the disc outskirts. Section 5.3 argues that our results are best explained by a true physical truncation of discs. Although the formalism presented thus far implies continual accretion limits the extent of discs, Section 5.4 considers other scenarios for limiting the extent of discs. Finally, we present some ancillary implications of our results in Section 5.5.

5.1 Spin parameter

Equation (10) is readily re-arranged to be

$$\lambda = \frac{\sqrt{50}}{\pi}\frac{t_{\rm orb}(R)}{t_{\rm H}}\frac{R_{\rm d}}{R}, \quad (11)$$

where $t_{\rm orb}(R)$ is the orbital time at radius R, and $t_{\rm H} = H_z^{-1}$ is the Hubble time (13.96 Gyr for our H_0), and assuming $j_{\rm d}/m_{\rm d} = 1$. Thus, spin parameter can be estimated from the orbital time at a given radius and the scaling of that radius with disc scalelength. Since $R_{\rm d}$ was not measured in our samples, indirect estimates of this scaling must be made. We do this using two approaches.

First, if all baryons are in an un-truncated exponential disc, we can use the SINGG results shown in Fig. 1 and Table 1 to estimate λ. Noting that the radius containing 50 per cent and 90 per cent of the light of such a disc corresponds to 1.68 and 3.89 times $R_{\rm d}$, and converting the mean orbital times in the log from Table 1, then we have $\lambda = 0.021$ and 0.020 estimated from $t_{\rm orb}(R_{50})$ and $t_{\rm orb}(R_{90})$, respectively. Being virtually identical, we take $\lambda = 0.020$ to be the average spin under the pure exponential disc assumption.

Secondly, we estimate $R_{\rm max}/R_{\rm d}$, and thus λ by scaling from the sample of Kregel et al. (2002) shown in Fig. 4b. They fit models including both an exponential disc and bulge to the light distribution of edge-on galaxies. Their disc model is truncated, yielding a maximum radius $R_{\rm max}$, which they find to be on average a factor 3.6 ± 0.6 times larger than $R_{\rm d}$. Their sample yields a significantly shorter average $t_{\rm orb} = 0.76$ Gyr than what we find, probably due to systematic differences in how $R_{\rm max}$ is determined. If so, then we scale their results to estimate

$$R_{\rm max} \sim (3.6 \pm 0.6)\frac{1}{0.76}R_{\rm d} = (4.7 \pm 0.8)R_{\rm d}. \quad (12)$$

Following equation (11), we have $\lambda = 0.034$ for $t_{\rm orb} = 1$ Gyr. Since this scales from an estimate that avoids bulges, it produces a longer $R_{\rm d}$ scalelength and hence higher λ value than assuming all the light comes from an exponential disc.

In comparison, measurements of typical average spin parameters of haloes created in cosmological simulations range from $\lambda = 0.03$ to 0.055, with each simulation set producing a broad distribution that is close to log normal and consistently found to have a width in the range $\sigma_{\log(\lambda)} \approx 0.21$–$0.23$ dex (Cole & Lacey 1996; Bullock et al. 2001; Bett et al. 2007; Macciò et al. 2007). Our first estimate, $\lambda = 0.020$ (assuming pure exponential discs), is somewhat below the expectations of cosmological simulations, whereas the second estimate $\lambda = 0.034$ (from scaling the results of Kregel et al. 2002) is at the low end of the expectations from simulations. The 0.23-dex difference in these estimates is indicative of the systematic uncertainty involved. In addition, neglection of the gaseous disc, or equivalently assuming the same distribution for it as the stars, will underestimate the angular momentum of the baryons, and thus λ. Improved estimates of λ can be made with better modelling of the baryonic mass and angular momentum distribution in galaxies (e.g. Obreschkow & Glazebrook 2014; Butler, Obreschkow & Oh 2017), but would still require assumptions about the coupling with the unseen DM halo. Our approach using equation (11) assumes a singular isothermal sphere and $j_{\rm d}/m_{\rm d} = 1$, both of which might introduce additional systematic bias in our estimate of λ.

Despite the likely systematic offset between our observational estimate of λ (via equation 11) and its true value, we can none the less discuss the relation between the *relative* scatter in $t_{\rm orb}$ and λ, or, equivalently, the absolute scatter in $\log t_{\rm orb}$ and $\log \lambda$. The observed scatter in $t_{\rm orb}(R_{\rm max})$ of ∼0.16 dex has several sources: (1) the physical dispersion in λ, (2) measurement uncertainties in $R_{\rm max}$ and $V_{\rm max}$, (3) variations in the ratio $R_{\rm max}/R_{\rm d}$, (4) variations in $j_{\rm d}/m_{\rm d}$, and (5) deviations from the assumed iso-thermal density profile. [3] We assume that (1) is the dominant source, but expect that the other sources make a non-negligible addition to the scatter of $t_{\rm orb}$. In Section 2, we (crudely) estimated (2) the scatter in $t_{\rm orb}$ due to measurement errors as 0.06 dex. Removing this (in quadrature), but neglecting (3), (4), and (5), the scatter in λ is $\sigma_{\log\lambda} \sim 0.15$ dex. This is somewhat lower than predicted by CDM models (0.23 dex; Macciò, Dutton & van den Bosch 2008). This is remarkable, given that we have not even accounted for the scatter of $t_{\rm orb}(R_{\rm max})$ coming from the sources (3), (4), and (5).

The explanation for the relatively low scatter in $t_{\rm orb}(R_{\rm max})$ is likely two-fold. First, to the extent that the disc surface mass density at $R_{\rm max}$ is similar in all galaxies, [4] high spin systems are likely to have their disc truncated at smaller radii relative to $R_{\rm d}$ than low-spin systems. Therefore, the scatter in $R_{\rm max}/R_{\rm d}$ (source 3) is negatively correlated to that of λ (source 1), hence *reducing* the scatter in $t_{\rm orb}(R_{\rm max})$, relative to the scatter in $t_{\rm orb}(R_{\rm d})$, which would be similar to the scatter in λ. R_{50} is the closest proxy we have to $R_{\rm d}$ and we do indeed find that the scatter in $t_{\rm orb}(R_{\rm max})$ is less than that of $t_{\rm orb}(R_{50})$ in both the optical and UV samples (Table 1). The effect is more prominent in the UV sample. Secondly, our sample is likely biased towards a more narrow range of spin parameters than present in a volume-complete sample of all DM haloes. The lowest λ haloes have little angular momentum and are more likely to be bulge dominated (i.e. S0 and elliptical galaxies); hence, they will have little H I, and not make it in to our samples. A rationale for our H I-selection producing a bias against high λ systems is less obvious. Effectively, all H I-selected galaxies are detected in the optical and UV (Meurer et al. 2006; Wong 2007); the detection limits are not biasing the samples. More speculatively, there may be a bias against high λ systems if the baryons they contain have not been able to cool enough for H I or stars to form.

5.2 Properties at disc galaxy outskirts

In Section 2, we defined $R_{\rm max}$ as the radius of readily detectable emission. It is largely determined by the amplitude of large-scale 'sky variations' in the *R* band (optical) and NUV (ultraviolet). These variations represent how well we can flat-field our data. The surface brightness of these variations provides a crude estimate of the limiting surface brightness at, or just interior to, $R_{\rm max}$. The situation is slightly different for $R_{\rm max}$(H I) – the limiting surface brightness is the measured $\Sigma_{\rm H\,I}$ at the last measured point in published H I profiles. Of course, a galaxy may extend beyond $R_{\rm max}$ at fainter levels than the limiting surface brightness. Histograms of limiting surface brightness are shown in Fig. 6.

The bottom axes of Fig. 6 show the limiting surface brightnesses converted to physically meaningful quantities. The *R*-band surface brightness $\mu_{\rm R}$ is converted to the stellar mass density $\Sigma_\star$, assuming a mass-to-light ratio $M/L_{\rm R} = 2\,{\rm M}_\odot/L_{{\rm R},\odot}$. For standard IMF assumptions, the adopted $M/L_{\rm R}$ is reasonable for a star-forming population, but probably will result in an underestimate for stellar mass densities if the relevant stellar population is old (Bell et al. 2003). To convert $\mu_{\rm NUV}$ to star formation intensity, we adopt the FUV conversion factor of Leroy et al. (2008) and assume an intrinsic colour $({\rm FUV}-{\rm NUV})_0 = 0$ ABmag, which is reasonable for the outer discs of galaxies (Gil de Paz et al. 2007; Thilker et al.

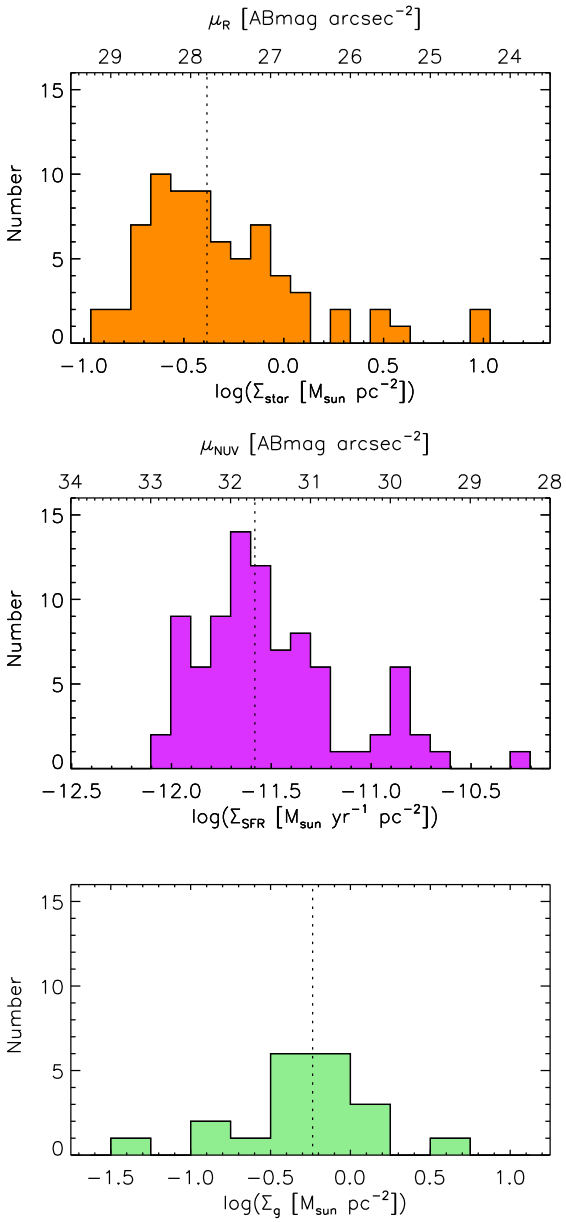

Figure 6. Histograms of limiting surface brightness in the *R* band and NUV for the SINGG and SUNGG samples are shown in the top and middle panels, respectively. The bottom panel shows the $\Sigma_{\rm gas}$ at the farthest point in the radial profiles of the galaxies in the H I sample, hence they correspond to the faintest H I recorded for each galaxy. The dotted vertical line in each panel shows the median of the distribution. The top axis on the top and middle panels gives the limiting surface brightness in observed units. The bottom axes are calibrated in physically meaningful quantities: stellar mass density ($\Sigma_\star$), star formation intensity (Σ_{SFR}), and H I surface mass density ($\Sigma_{\rm gas}$) for the top, middle, and bottom panels, respectively.

[3] This includes variations in the ratio of circular velocity measured over the disc to that at the virial radius, V/V_{200}.

[4] In Section 5.2, we show that the surface brightness limits at $R_{\rm max}$ varies greatly, but this does not preclude the corresponding mass densities just interior to where this limit is found to be similar.

2007; Zaritsky & Christlein 2007; Boissier et al. 2008; Goddard, Kennicutt & Ryan-Weber 2010; Hunter, Elmegreen & Ludka 2010; Werk et al. 2010a; Lee et al. 2011). The ISM density Σ_g assumes that the ISM is dominated by H I and is corrected by a factor of 1.3 to account for heavier elements.

The medians of the distributions are marked in Fig. 6 and correspond to $\Sigma_\star = 0.42\,M_\odot\,pc^{-2}$, $\Sigma_{SFR} = 2.8\times10^{-12}M_\odot\,yr^{-1}\,pc^{-2}$, and $\Sigma_g = 0.58\,M_\odot\,pc^{-2}$. These may be considered typical conditions at or near R_{max}. The star formation intensity at R_{max} is weak compared to the stellar and gaseous contents. The time needed to form the observed stellar populations at the current star formation intensity is $t_{build} = \Sigma_\star/\Sigma_{SFR} = 150$ Gyr, whereas the time required to process the gas through star formation is $t_g = \Sigma_g/\Sigma_{SFR} \sim 200$ Gyr. Equivalently, both the specific star formation rate (t_{build}^{-1}) and the star formation efficiency (t_g^{-1}) are low in outer discs. Thus, at R_{max}, the current *in situ* star formation is too feeble to either create the stellar populations or transform the accumulated ISM into stars in a reasonable amount of time.

For a galaxy to have the same R_{max} in the R band, the NUV implies that the NUV-R colour at R_{max} is similar to the -'colour-' of the large-scale sky fluctuations, i.e. NUV-R $\approx \mu_{sky}$(NUV) $-$ $\mu_{sky}(R) \approx 3.8$ ABmag. This is a 'green-valley' colour, i.e. intermediate between the blue and red sequences (Schiminovich et al. 2007), validating the long t_{build} we derive above.

The slope of the RV relationship in the R band ($\beta_{optical} = 1.13 \pm 0.06$) is slightly steeper than in the NUV ($\beta_{UV} = 1.04 \pm 0.06$). A comparison between Figs 1 and 2 shows that the values of R_{max} in the optical and UV are nearly equal to that at the high end, where $V \gtrsim 200\,km\,s^{-1}$, whereas for $V \lesssim 50 km\,s^{-1}$, we find that, on average, galaxies have $R_{max}(R) \lesssim 0.7R_{max}$(NUV). Hence, at R_{max}(NUV), galaxies are redder for large spirals than dwarfs. This may be due to the relative importance of an old component in the disc or halo for spirals compared to dwarfs. It may also be a sign of 'downsizing' that lower mass galaxies are less evolved into stars than high-mass galaxies.

5.3 The edge of the disc

Our results imply a distinct physical edge in the light distribution corresponding to R_{max}. The first line of evidence for this is the result that the three tracers give nearly identical estimates of t_{orb}; for a given V_{max} they yield the same radius in the distribution of stars, star formation, and atomic hydrogen. If discs were purely exponential, then the equality in t_{orb} would be remarkably coincidental, since the different measurements of R_{max} are set by independent observational limits for each tracer. If the observational limits were consistent within each band, then one could argue that R_{max} is effectively an isophotal radius. Previous studies (Saintonge et al. 2008; Saintonge & Spekkens 2011; Hall et al. 2012) have shown that isophotal radii produce tighter RV relationships than those using an exponential scalelength, perhaps because of the difficulty in consistently measuring R_d in the face of contamination from the bulge, breaks in radial profiles, and biases in setting the range of radii to fit with an exponential (Freeman 1970; Pohlen & Trujillo 2006; Hall et al. 2012; Zheng et al. 2015). However, as shown by Fig. 6, the limiting surface brightness is not consistent between galaxies, hence R_{max} is not an isophotal radius.

Indeed, the observed scatter in the RV relationship provides a second line of evidence that we are dealing with a truncation in the disc. The dispersion in limiting surface brightnesses shown in Fig. 6 is 0.40, 1.05, and 0.44 dex in the R band, NUV, and H I, respectively. Assuming a pure exponential disc and adopting equation (12) for the mean scaling between the disc scalelength and R_{max}, these dispersions should contribute 0.08, 0.27, and 0.09 dex to the respective scatter in the RV relationships, whereas the corresponding observed scatters are 0.15, 0.16, and 0.18 dex. Thus, the expected induced scatter, in this scenario, is larger than the observed scatter in the NUV, whereas it would make a considerable fraction (~25 per cent in quadrature) of the observed scatter in the R band and H I.

That we are seeing a real edge to the disc is most apparent in the H I sample. Using the data from MZD13, we find an average power-law index $\gamma = -4.6 \pm 0.5$ for $\Sigma_{HI}(R)$ profiles between R_2 and (H I) (the uncertainty is the standard error on the mean). If this slope is maintained towards larger R, the total H I content is well constrained. This is unlike the region R_1 to R_2, where the H I traces DM well but $\gamma \approx -1$, which cannot be maintained indefinitely. Modern H I observations are sufficiently deep that large improvements in sensitivity of observations do not result in large changes to the H I content. For example, Gentile et al. (2013) present HALOGAS survey data of NGC 3198 with an H I surface brightness sensitivity 10 times fainter than the THINGS observations used by MZD13. Those improved observations result in an increase of 6 per cent in the H I flux, and 21 per cent (0.08 dex) in maximum radius compared to the THINGS data.

We conclude that discs are not purely exponential all the way to R_{max}, but must have a steep fall-off in surface brightness near R_{max}. An edge, or steep fall-off, in surface brightness has been noted in the optical by van der Kruit and collaborators (van der Kruit 2007; Kregel et al. 2002) and in H I by van Gorkom (1993). Our results are similar to theirs (Fig. 4), indicating that disc has nearly identical truncations at R_{max} in stars, star formation, and atomic hydrogen, and that it is this physical disc truncation that we are observing.

Baryons clearly exist beyond R_{max} in galaxies. For example, at the rotational amplitude of our Galaxy $V = 220\,km\,s^{-1}$, then $t_{orb} = 1$ Gyr corresponds to $R_{max} = 33$ kpc. The RC of the Milky Way disc can be traced out to $R \approx 20$ kpc (Sofue, Honma & Omodaka 2009; Burch & Cowsik 2013; Bhattacharjee, Chaudhury & Kundu 2014), whereas halo blue horizontal branch stars can be detected out to $R \approx 60$ kpc (Xue et al. 2008) and globular clusters out to $R \approx 100$ kpc (e.g. Pal 3; Koch, Côté & McWilliam 2009). In M31, the stellar disc can be traced to at least $R = 40$ kpc as shown by Ibata et al. (2005). Using their adopted RC (Klypin, Zhao & Somerville 2002), $t_{orb} = 1.04$ Gyr at this radius, nicely consistent with our average t_{orb} at R_{max}. Ibata et al. (2005) point out that additional fainter disc material may be detected out to 70 kpc, whereas Ibata et al. (2014) show faint but prominent features at larger radii relate to the halo, which extends to at least 150 kpc, about half the virial radius of $R_{vir} \approx 290$ kpc (Klypin et al. 2002). Clearly there are stars well beyond where t_{orb} is 1 Gyr in both the Milky Way and M31. But they are primarily located in their host's halo, rather than disc.

5.4 Alternative mechanisms to truncate discs

The cosmological approach we adopted in Section 5.1 implies that discs grow with cosmic time (the H_z^{-1} dependence) due to accretion. Disc growth is also predicted in simple semi-analytic model extensions to cosmological N-body simulations, albeit with weaker growth (Dutton et al. 2011). However, other mechanisms may also be at play in setting the extent of galactic discs. These include the limitations in the angular momentum in an initial protogalactic collapse (van der Kruit 1987), truncation in star formation due to disc stabilization (Kennicutt 1989; Martin & Kennicutt 2001), ionization by the ultraviolet background (UVB; van Gorkom 1993), and

spreading of the disc due to internal angular momentum transfer (Roškar et al. 2008a,b).

The fact that we see the linear *RV* expected for the cosmological accretion scenario is a strong argument in its favour. Likewise, simple semi-analytic models of galaxy evolution that incorporate accretion can account for the redshift evolution of the *RV* relationship and other virial scaling relations (Dutton et al. 2011). However, 'smoking-gun' observations of intergalactic gas being 'caught in the act' of accreting on to galaxies have been elusive. In a naive interpretation of the accretion scenario, one would expect outer discs to be largely gaseous. Instead, the equality of $t_{\rm orb}$ in the *R* band and H I combined with the near equality of $\Sigma_{\rm H\,I}$ and Σ_* in the outer discs implied by Fig. 6 suggests that they are well evolved in to stars (albeit typically less so than inner disc). This conclusion should be considered tentative since our methods for estimating the various $R_{\rm max}$ values as well as $\Sigma_{\rm H\,I}$ and Σ_* are crude.

An older scenario for producing a truncated but evolved outer disc is the concept of a rapid initial collapse of galaxies including their discs (Eggen, Lynden-Bell & Sandage 1962; Freeman 1970). van der Kruit (1987) shows that an initial uniformly rotating spherical gas cloud in a potential with a flat RC that collapses while conserving angular momentum will produce an exponential disc that truncates at 4.5 times the disc scalelength. In practise, Kregel et al. (2002) found that stellar discs truncate at $R_{\rm max} \sim 3.6R_{\rm d}$, i.e. somewhat smaller. However, as argued in Section 5.2, they are likely measuring shorter $R_{\rm max}$ values than we do. Indeed, van der Kruit (2007) notes that the truncations examined by Kregel et al. (2002) correspond to $\mu_V \sim 26.5$–27.5 mag arcsec^{-2}, brighter than our estimates of the surface brightness at $R_{\rm max}$ (Fig. 6). The fact that van der Kruit (2007) often find H I beyond their optical truncation radii is consistent with them underestimating $R_{\rm max}$ compared to us, since our H I and optical $R_{\rm max}$ values are consistent. When we scale their results to our $t_{\rm orb}$(equation 12), we find that the ratio between $R_{\rm d}$ and $R_{\rm max}$ is a factor of 4.7 ± 0.8, consistent with what is expected from a monolithic early collapse.

Kennicutt (1989) note that star formation, as traced by H II regions in spiral galaxies, typically cuts off at a radius $R_{\rm HII}$, beyond which few bright H II regions are detected. Martin & Kennicutt (2001) confirmed this result with improved observations of more galaxies. Fig. 4 b plots $R_{\rm HII}$ for five galaxies from Martin & Kennicutt (2001), which are also in the sample of MZD13. The $R_{\rm HII}$ values (which correspond to $t_{\rm orb} = 48$ to 390 Myr) are considerably smaller than the $R_{\rm max}$ values in our primary samples, but similar to the break radius $R_{\rm b}$ of the PS1 sample. Christlein, Zaritsky & Bland-Hawthorn (2010) find that the H α distribution of edge-on spirals typically has a downward break at $0.7R_{90}(R)$, which, they note, may correspond to the $R_{\rm HII}$ break. This scaling is very close to the $R_{\rm b} \approx 0.8R_{90}$ scaling we find for the PS1 sample, strengthening the notion that $R_{\rm b}$ and $R_{\rm HII}$ are related. The fact that Christlein et al. (2010) find H α emission beyond their break radius and the SUNGG UV measurements continue out to $\sim$2.2$R_{90}(R)$ demonstrates that the limits of galaxies traced by prominent H II regions does not measure the full extent of star formation in galactic discs.

Instead, UV emission is a better tracer of star formation in outer discs. The existence of extended UV (XUV) discs (Gil de Paz et al. 2005; Thilker et al. 2005, 2007) demonstrates that star formation can extend beyond the portion of the disc readily observed in the optical. These outer discs can also be probed using resolved stellar populations from the ground (Cuillandre et al. 2001; Ibata et al. 2005) or space (e.g. Bruzzese et al. 2015). The close match in the *RV* relationships at $R_{\rm max}$ shown in Fig. 4 implies that star formation extends to the limits of the H I disc.

One mechanism that has been promoted for limiting the extent of galaxy discs is ionization by the UVB posited by van Gorkom (1993) to explain the steep decline in $\Sigma_{\rm H\,I}$ profiles at large *R* in NGC 3198 and other galaxies. The scenario was consistent with modelling of the time (Maloney 1993). The column densities he considered are similar to or somewhat smaller than the typical $\Sigma_{\rm H\,I} \sim 0.1\,\mathcal{M}_\odot$ pc^{-2} we find at $R_{\rm max}$(H I). If ionized by the background is setting $R_{\rm max}$(H I) then one should be able to detect emission from the ionized disc beyond $R_{\rm max}$. Bland-Hawthorn, Freeman & Quinn (1997) present evidence for finding this emission in the outer disc of NGC 253. However, other searches for ionized disc gas beyond the H I edges of galaxies have not been successful (e.g. Madsen et al. 2001; Dicaire et al. 2008; Adams et al. 2011; Hlavacek-Larrondo et al. 2011). Recent very deep integral field spectroscopy of the outermost disc of UGC 7321 finds very low surface brightness H α, consistent with ionization by the UVB, but this emission does not extend beyond the $\Sigma_{\rm H\,I} \sim 0.1\,\mathcal{M}_\odot$ pc^{-2} contour (Fumagalli et al. 2017). Although UVB may ionize the 'skin' of H I discs, ionization gas does not extend much beyond the observable H I disc, which marks the true maximum extent of the cool ISM disc.

Roškar et al. (2008a,b) model the interplay between star formation and disc dynamics in isolated spiral galaxies. Their simulations produce star formation edges like that seen by Kennicutt (1989) and Martin & Kennicutt (2001), beyond which the gaseous part of the disc has a high Toomre (1964) disc stability parameter *Q* and thus produces little *in situ* star formation. Instead, most of the old stars at large radii formed at smaller radii and 'migrated' outwards due to resonances with transient spiral features. Such a process can explain the downward breaking surface brightness profiles, 'U' shaped age, and colour profiles commonly seen in spiral galaxies (e.g. Pohlen & Trujillo 2006; Bakos & Trujillo 2013; Zheng et al. 2015). The material in discs between $R_{\rm HII}$ and $R_{\rm max}$ may then be a combination of weak XUV disc star formation in the *Q* stable portion of the disc combined with outwardly migrating older stars. Although this scenario is appealing, it is not obvious how it would result in a linear *RV* relation largely consistent at different wavelengths down to the dwarf galaxy regime. Low-mass galaxies are also a concern because they do not have spiral density waves that are likely to drive radial migrations.

5.5 Other implications

There is a strong relationship between the H I radius and H I mass in galaxies of the form

$$M_{\rm H\,I} \propto R_{\rm H\,I}^2. \tag{13}$$

This was emphasized recently by Wang et al. (2016), who note that it has been found for samples selected in a wide variety of ways (Broeils & Rhee 1997; Verheijen & Sancisi 2001; Swaters et al. 2002; Noordermeer et al. 2005; Wang et al. 2013). The correlation implies that the average H I surface brightness within $R_{\rm H\,I}$ is constant. The scatter in this relationship is $\sim$0.06 dex, tighter than our *RV* relationship. The *RV* relationship at $R_{\rm max}$ is peripherally related to this result. It has long been known that a maximum $\Sigma_{\rm H\,I} \sim 10\,\mathcal{M}_\odot$ pc^{-2} is set by the conversion of the interstellar medium into a molecular form (e.g. Bigiel et al. 2008), and many galaxies reach this saturation in their central regions. The outer radius adopted by Wang et al. (2016) is where $\Sigma_{\rm H\,I} = 1\,\mathcal{M}_\odot$ pc^{-2} brighter than adopted for our H I sample (MZD13). This effectively limits the range of allowed average surface brightness. Within galaxies, H I has a predictable distribution giving a power-law fall-off in

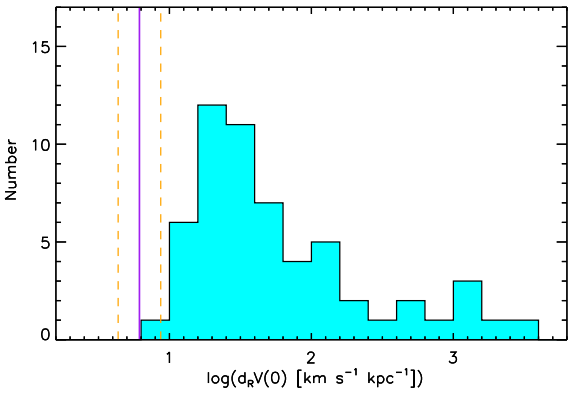

Figure 7. Histogram of central velocities gradients of a wide range of disc galaxies from the sample of Lelli, Fraternali & Verheijen (2013). The solid vertical line marks the velocity gradient equivalent to the mean orbital time $t_{\rm orb} = 1$ Gyr at $R_{\rm max}$ of our samples, whereas the dashed lines indicate the dispersion about this mean time of 0.16 dex. Galaxies do not have central densities less than $\rho = 2.1 \times 10^{-3}\,\mathcal{M}_\odot\,{\rm pc}^{-3}$.

$\Sigma_{\rm H\,I}$, which is apparently set by the disc maintaining a constant stability parameter (Meurer et al. 2013; Wong et al. 2016). The limited dynamic range of $\Sigma_{\rm H\,I}$, combined with the shallow power-law radial profile, results in the narrow range of average $\Sigma_{\rm H\,I}$.

Since radial density profiles typically decrease monotonically with R, the central density should not be less than the average density at $R_{\rm max}$. This corresponds to a constraint on the slope of the inner RC of galaxies – the gradient should not be less than that implied by the *RV* relation at $R_{\rm max}$, hence the orbital time should be less than or equal to $\sim$1 Gyr in the central parts of galaxies. Fig. 7 tests this assertion by plotting the histogram of central velocity gradients, $d_R V(0)$, for 57 galaxies comprising the final sample of Lelli et al. (2013) with valid measurements. The dashed line shows the gradient $d_R V(0) = 6.1\,{\rm km\,s^{-1}\,kpc^{-1}}$ corresponding to $t_{\rm orb} = 1$ Gyr. There are no galaxies with a shallower gradient. The shallowest $d_R V(0) = 9.0\,{\rm km\,s^{-1}\,kpc^{-1}}$ in their sample corresponds to the irregular galaxy IC 2574 (de Blok et al. 2008). Following the discussion in Sections 4 and 5, a galaxy with a central density less than $\langle\rho(R_{\rm max})\rangle$ would have had to have collapsed less than our samples, and that would mean they either have a higher λ or $j_{\rm d}/m_{\rm d} > 1$ (i.e. they have a larger fraction of the spin in the disc than the fraction of mass in the disc) or some combination of the two. Apparently, such galaxies have not (yet) formed.

6 CONCLUSIONS

We have shown that disc galaxies display a nearly linear radius–velocity (*RV*) relationship at the outermost radius $R_{\rm max}$ observed in the optical, UV, and H I emission at 21cm. The *RV* relationship is consistent between data sets and implies a constant orbital time of $\sim$1 Gyr at this radius. A comparison of our H I-selected and optically measured SINGG sample with the much larger optically selected and measured PS1 sample of Zheng et al. (2015) shows nearly identical *RV* relations at two fiducial radii. This suggests that our results are robust against the vagaries of sample selection and may be generic to disc galaxies in the low-redshift Universe. Within $R_{\rm max}$, matter has collapsed by a factor of 37 to $\rho_M = 2.1 \times 10^{-3}\,\mathcal{M}_\odot\,{\rm pc}^{-2}$, a factor of 4.9×10^4 times higher than the present day average matter density in the Universe.

We argue that $R_{\rm max}$ in our data sets corresponds to the edge of the disc. Recent studies indicate that $R_{\rm max}$(H I) is limited by the available ISM in the disc rather than external ionization by the UVB. The star formation intensity at $R_{\rm max}$ is an order of magnitude too weak to build up the existing stellar populations or consume the available gas within a Hubble time. Hence, star formation at its current rate is not solely responsible for setting this radius. Although $R_{\rm max}$ appears to mark a sharp truncation in the disc of galaxies, it does not enclose all baryons. Stars in the halo are distributed to much larger radii, and their kinematics indicate the DM also extends further, likely to the virial radius.

Instead, $R_{\rm max}$ must be set by other processes such as accretion (e.g. Sancisi et al. 2008; Brook et al. 2012; Mollá et al. 2016). Continuous cosmic accretion provides a natural explanation for the *RV* relation. In that scenario, the *RV* relation gives a constraint on the average spin parameter, which we estimate to be in the range $\lambda = 0.02$–0.035. This estimate is likely to be biased due to the crudeness of our estimates and the requirement for H I in our samples, which will bias them against the typically gas poor and low spin elliptical and S0 galaxies. The scatter in the orbital times provides a constraint on the dispersion of spin parameters $\sigma_{\log(\lambda)} \approx 0.16$ dex, somewhat smaller than expected by theory ($\sim$0.22 dex), probably also due in part to the previously mentioned biases. The scatter in orbital times may also underestimate that in λ if $R_{\rm max}$ corresponds to a consistent disc surface brightness or mass density.

An older theory, consistent with our results, is that $R_{\rm max}$ is set by a rapid early collapse. Unfortunately, this scenario does not make a prediction on the *RV* relationship. However, a crude estimate of the scaling of $R_{\rm max}$ with disc scalelength $R_{\rm d}$ (following the results of Kregel et al. 2002) is consistent with long-standing theoretical predictions for this scenario ($R_{\rm max}/R_{\rm d} \sim 4.5$ van der Kruit 1987). Our estimates of the gas and stellar surface densities near $R_{\rm max}$ are very similar, indicating a high degree of evolution of outer discs. The relatively flat metallicity gradients in the outskirts of galaxies also indicates a high degree of chemical evolution in disc outskirts (Werk et al. 2010b, 2011). Hence, an early rapid collapse model is nominally consistent with our results. However, our estimates of $R_{\rm max}/R_{\rm d}$ and the surface densities at $R_{\rm max}$ are crude. Better estimates are needed to test this interpretation.

The *RV* relationship has some practical implications. Since the conversion of angular to physical radius is distance dependent, whereas the conversion of velocities is not (to first order), then one could use our *RV* relationship to estimate distances. However, since the observed relationship is linear it is not as powerful as the TFR where luminosity goes as orbital velocity to a power of three to four (e.g. Meyer et al. 2008). Furthermore, due to the likely evolution in this relationship (Dutton et al. 2011), one must take care to limit its use to the local Universe.

A simple *RV* scaling relation provides a convenient tool to estimate the extent of galaxy discs. We used the $R_{\rm max}$ found here in the model we developed to explain the nearly constant ratio of star formation rate (as traced in the UV) to the H I mass (Wong et al. 2016). Further development of this model would be useful for determining a wide range of properties along the star-forming main-sequence of galaxies. Of particular relevance would be using such an approach, combined with observed column density distributions within galaxies, to model the likely cross-section of H I absorbers (e.g. Rao & Briggs 1993; Ryan-Weber, Webster & Staveley-Smith 2003, 2005; Zwaan et al. 2005; Braun 2012). Similarly a realistic disc truncation radius could be usefully employed in setting the initial conditions for detailed dynamical simulations of local galaxies, or for modelling the inclusion of baryons in semi-analytic models.

ACKNOWLEDGEMENTS

GRM acknowledges useful discussions with Tim Heckman, Brent Tully, Ken Freeman, Joss Bland-Hawthorn, Emma Ryan-Weber, and Martin Zwaan. GRM also thanks the Center for Astrophysical Sciences of the Johns Hopkins University, and the National Astronomical Observatories of the Chinese Academy of Sciences for their hospitality during visits while this paper was being developed. ZZ is supported by the National Natural Science Foundation of China Grant No. 11703036. Partial funding for the SINGG and SUNGG surveys came from National Aeronautics and Space Administration (NASA) grants NAG5-13083 (Long-Term Space Astrophysics program), *GALEX* GI04-0105-0009 (NASA *GALEX* Guest Investigator grant), and NNX09AF85G (*GALEX* archival grant) to GRM. The SINGG observations were made possible by a generous allocation of time from the Survey Program of the National Optical Astronomy Observatory (NOAO), which is operated by the Association of Universities for Research in Astronomy (AURA), Inc., under a cooperative agreement with the National Science Foundation. *GALEX* is a NASA Small Explorer, launched in 2003 April. We gratefully acknowledge NASA's support for construction, operation, and science analysis for the *GALEX* mission, developed in cooperation with the Centre National d'Etudes Spatiales of France and the Korean Ministry of Science and Technology. This research has made use of the NASA/IPAC Extragalactic Database (NED), which is operated by the Jet Propulsion Laboratory, California Institute of Technology, under contract with the National Aeronautics and Space Administration.

REFERENCES

Adams J. J., Uson J. M., Hill G. J., MacQueen P. J., 2011, Ap&SS, 728, 107
Bakos J., Trujillo I., 2013, Mem. Soc. Astron. Italiana Sup., 25, 21
Bell E. F., McIntosh D. H., Katz N., Weinberg M. D., 2003, ApJS, 149, 289
Bett P., Eke V., Frenk C. S., Jenkins A., Helly J., Navarro J., 2007, MNRAS, 376, 215
Bhattacharjee P., Chaudhury S., Kundu S., 2014, Ap&SS, 785, 63
Bigiel F., Leroy A., Walter F., Brinks E., de Blok W. J. G., Madore B., Thornley M. D., 2008, AJ, 136, 2846
Bland-Hawthorn J., Freeman K. C., Quinn P. J., 1997, Ap&SS, 490, 143
Boissier S. et al., 2008, ApJ, 681, 244
Bonoli S., Mayer L., Kazantzidis S., Madau P., Bellovary J., Governato F., 2016, MNRAS, 459, 2603
Bosma A., 1981, AJ, 86, 1825
Braun R., 2012, Ap&SS, 749, 87
Broeils A. H., Rhee M.-H., 1997, A&A, 324, 877
Brook C. B. et al., 2012, MNRAS, 426, 690
Bruzzese S. M., Meurer G. R., Lagos C. D. P., Elson E. C., Werk J. K., Blakeslee J. P., Ford H., 2015, MNRAS, 447, 618
Bullock J. S., Dekel A., Kolatt T. S., Kravtsov A. V., Klypin A. A., Porciani C., Primack J. R., 2001, Ap&SS, 555, 240
Burch B., Cowsik R., 2013, Ap&SS, 779, 35
Butler K. M., Obreschkow D., Oh S.-H., 2017, ApJ, 834, L4
Calzetti D., Kinney A. L., Storchi-Bergmann T., 1994, Ap&SS, 429, 582
Cappellari M. et al., 2012, Nature, 484, 485
Catinella B., Giovanelli R., Haynes M. P., 2006, ApJ, 640, 751
Chambers K. C. et al., 2016, MNRAS, submitted
Christlein D., Zaritsky D., Bland-Hawthorn J., 2010, MNRAS, 405, 2549
Cole S., Lacey C., 1996, MNRAS, 281, 716
Conroy C., van Dokkum P. G., 2012, Ap&SS, 760, 71
Courteau S., Dutton A. A., van den Bosch F. C., MacArthur L. A., Dekel A., McIntosh D. H., Dale D. A., 2007, ApJ, 671, 203
Cuillandre J.-C., Lequeux J., Allen R. J., Mellier Y., Bertin E., 2001, Ap&SS, 554, 190
de Blok W. J. G., Walter F., Brinks E., Trachternach C., Oh S.-H., Kennicutt R. C., 2008, AJ, 136, 2648
Dicaire I., Carignan C., Amram P., Marcelin M., Hlavacek-Larrondo J., de Denus-Baillargeon M. M., Daigle O., Hernandez O., 2008, AJ, 135, 2038
Dutton A. A., van den Bosch F. C., Dekel A., Courteau S., 2007, Ap&SS, 654, 27
Dutton A. A. et al., 2011, MNRAS, 410, 1660
Dutton A. A., Mendel J. T., Simard L., 2012, MNRAS, 422, L33
Eggen O. J., Lynden-Bell D., Sandage A. R., 1962, ApJ, 136, 748
Epinat B. et al., 2008, MNRAS, 388, 500
Fall S. M., Efstathiou G., 1980, MNRAS, 193, 189
Freeman K. C., 1970, ApJ, 160, 811
Fumagalli M., Haardt F., Theuns T., Morris S. L., Cantalupo S., Madau P., Fossati M., 2017, MNRAS, 467, 4802
Gentile G. et al., 2013, A&A, 554, A125
Gil de Paz A. et al., 2005, ApJ, 619, L29
Gil de Paz A. et al., 2007, ApJS, 173, 185
Goddard Q. E., Kennicutt R. C., Ryan-Weber E. V., 2010, MNRAS, 405, 2791
Gordon K. D., Misselt K. A., Witt A. N., Clayton G. C., 2001, Ap&SS, 551, 269
Governato F. et al., 2010, Nature, 463, 203
Graham A. W., Driver S. P., Petrosian V., Conselice C. J., Bershady M. A., Crawford S. M., Goto T., 2005, AJ, 130, 1535
Grebel E. K., 1997, Rev. Mod. Astron., 10, 29
Gunawardhana M. L. P. et al., 2011, MNRAS, 415, 1647
Hall M., Courteau S., Dutton A. A., McDonald M., Zhu Y., 2012, MNRAS, 425, 2741
Hlavacek-Larrondo J., Marcelin M., Epinat B., Carignan C., de Denus-Baillargeon M. M., Daigle O., Hernandez O., 2011, MNRAS, 416, 509
Hoversten E. A., Glazebrook K., 2008, Ap&SS, 675, 163
Hubble E. P., 1926, ApJ, 64, 321
Hunter D. A., Elmegreen B. G., Ludka B. C., 2010, AJ, 139, 447
Ibata R., Chapman S., Ferguson A. M. N., Lewis G., Irwin M., Tanvir N., 2005, Ap&SS, 634, 287
Ibata R. A. et al., 2014, Ap&SS, 780, 128
Isobe T., Feigelson E. D., Akritas M. G., Babu G. J., 1990, ApJ, 364, 104
Kauffmann G. et al., 2003, MNRAS, 341, 54
Kennicutt R. C., 1989, ApJ, 344, 685
Klypin A., Zhao H., Somerville R. S., 2002, Ap&SS, 573, 597
Koch A., Côté P., McWilliam A., 2009, A&A, 506, 729
Koribalski B. S. et al., 2004, AJ, 128, 16
Kregel M., van der Kruit P. C., de Grijs R., 2002, MNRAS, 334, 646
Lee J. C. et al., 2009, Ap&SS, 706, 599
Lee J. C. et al., 2011, ApJS, 192, 6
Lelli F., Fraternali F., Verheijen M., 2013, MNRAS, 433, L30
Leroy A. K., Walter F., Brinks E., Bigiel F., de Blok W. J. G., Madore B., Thornley M. D., 2008, AJ, 136, 2782
Macciò A. V., Dutton A. A., van den Bosch F. C., Moore B., Potter D., Stadel J., 2007, MNRAS, 378, 55
Macciò A. V., Dutton A. A., van den Bosch F. C., 2008, MNRAS, 391, 1940
Madsen G. J., Reynolds R. J., Haffner L. M., Tufte S. L., Maloney P. R., 2001, Ap&SS, 560, L135
Maloney P., 1993, ApJ, 414, 41
Martin C. L., Kennicutt R. C., 2001, Ap&SS, 555, 301
Mathewson D. S., Ford V. L., Buchhorn M., 1992, ApJS, 81, 413
McGaugh S. S., Schombert J. M., Bothun G. D., De Blok W., 2000, ApJ, 533, L99
Meurer G. R. et al., 2006, ApJS, 165, 307
Meurer G. R. et al., 2009, Ap&SS, 695, 765
Meurer G. R., Zheng Z., de Blok W. J. G., 2013, MNRAS, 429, 2537 (MZD13)
Meyer M. J. et al., 2004, MNRAS, 350, 1195
Meyer M. J., Zwaan M. A., Webster R. L., Schneider S., Staveley-Smith L., 2008, MNRAS, 391, 1712
Mo H. J., Mao S., White S. D. M., 1998, MNRAS, 295, 319 (MMW98)

Mollá M., Díaz Á. I., Gibson B. K., Cavichia O., López-Sánchez Á.-R., 2016, MNRAS, 462, 1329
Navarro J. F., Frenk C. S., White S. D. M., 1997, Ap&SS, 490, 493
Noordermeer E., van der Hulst J. M., Sancisi R., Swaters R. A., van Albada T. S., 2005, A&A, 442, 137
Obreschkow D., Glazebrook K., 2014, Ap&SS, 784, 26
Oh S.-H., Brook C., Governato F., Brinks E., Mayer L., de Blok W. J. G., Brooks A., Walter F., 2011, AJ, 142, 24
Persic M., Salucci P., 1991, ApJ, 368, 60
Persic M., Salucci P., Stel F., 1996, MNRAS, 281, 27
Petrosian V., 1976, ApJ, 209, L1
Planck Collaboration XVI, 2014, A&A, 571, A16
Pohlen M., Trujillo I., 2006, A&A, 454, 759
Posti L., Pezzulli G., Fraternali F., di Teodoro E., 2018, MNRAS, 475, 232
Rao S., Briggs F., 1993, ApJ, 419, 515
Reyes R., Mandelbaum R., Gunn J. E., Pizagno J., Lackner C. N., 2011, MNRAS, 417, 2347
Roškar R., Debattista V. P., Stinson G. S., Quinn T. R., Kaufmann T., Wadsley J., 2008a, Ap&SS, 675, L65
Roškar R., Debattista V. P., Quinn T. R., Stinson G. S., Wadsley J., 2008b, Ap&SS, 684, L79
Rubin V. C., Thonnard N., Ford W. K. J., 1978, ApJ, 225, L107
Ryan-Weber E. V., Webster R. L., Staveley-Smith L., 2003, MNRAS, 343, 1195
Ryan-Weber E. V., Webster R. L., Staveley-Smith L., 2005, MNRAS, 356, 1600
Saintonge A., Spekkens K., 2011, ApJ, 726, 77
Saintonge A., Masters K. L., Marinoni C., Spekkens K., Giovanelli R., Haynes M. P., 2008, A&A, 478, 57
Sancisi R., Fraternali F., Oosterloo T., van der Hulst T., 2008, A&AR, 15, 189
Schiminovich D. et al., 2007, ApJS, 173, 315
Sérsic J. L., 1963, Bole. Asociacion Argentina de Astron., 6, 41
Simons R. C., Kassin S. A., Weiner B. J., Heckman T. M., Lee J. C., Lotz J. M., Peth M., Tchernyshyov K., 2015, MNRAS, 452, 986
Smith R. J., Lucey J. R., Carter D., 2012, MNRAS, 426, 2994
Sofue Y., Honma M., Omodaka T., 2009, PASJ, 61, 227
Swaters R. A., van Albada T. S., van der Hulst J. M., Sancisi R., 2002, A&A, 390, 829
Thilker D. A. et al., 2005, Ap&SS, 619, L79
Thilker D. A. et al., 2007, ApJS, 173, 538
Tolstoy E., Hill V., Tosi M., 2009, ARA&A, 47, 371
Toomre A., 1964, ApJ, 139, 1217
Treu T., Auger M. W., Koopmans L. V. E., Gavazzi R., Marshall P. J., Bolton A. S., 2010, Ap&SS, 709, 1195
Tuffs R. J., Popescu C. C., Völk H. J., Kylafis N. D., Dopita M. A., 2004, A&A, 419, 821
Tully R. B., Fisher J. R., 1977, A&A, 54, 661
van der Kruit P. C., 1987, A&A, 173, 59
van der Kruit P. C., 2007, A&A, 466, 883
van Dokkum P. G., Conroy C., 2012, Ap&SS, 760, 70
van Gorkom J., 1993, in Shull J., Thronson H., eds, The Environment and Evolution of Galaxies. Kluwer, Dordrecht, p. 345
Verheijen M. A. W., Sancisi R., 2001, A&A, 370, 765
Wang J. et al., 2013, MNRAS, 433, 270
Wang J., Koribalski B. S., Serra P., van der Hulst T., Roychowdhury S., Kamphuis P., Chengalur J. N., 2016, MNRAS, 460, 2143
Weisz D. R. et al., 2011, Ap&SS, 739, 5
Werk J. K. et al., 2010a, AJ, 139, 279
Werk J. K., Putman M. E., Meurer G. R., Thilker D. A., Allen R. J., Bland-Hawthorn J., Kravtsov A., Freeman K., 2010b, Ap&SS, 715, 656
Werk J. K., Putman M. E., Meurer G. R., Santiago-Figueroa N., 2011, Ap&SS, 735, 71
Williams B. F. et al., 2011, ApJ, 734, L22
Wong O. I., 2007, PhD Thesis, University of Melbourne
Wong O. I., Meurer G. R., Zheng Z., Heckman T. M., Thilker D. A., Zwaan M. A., 2016, MNRAS, 460, 1106
Xue X. X. et al., 2008, Ap&SS, 684, 1143
Zaritsky D., Christlein D., 2007, AJ, 134, 135
Zheng Z. et al., 2015, Ap&SS, 800, 120
Zwaan M. A. et al., 2004, MNRAS, 350, 1210
Zwaan M. A., van der Hulst J. M., Briggs F. H., Verheijen M. A. W., Ryan-Weber E. V., 2005, MNRAS, 364, 1467

This paper has been typeset from a TEX/LATEX file prepared by the author.